JACS
JOURNAL OF THE AMERICAN CHEMICAL SOCIETY
Communication
Cite This: J. Am. Chem. Soc. 2017, 139, 16060-16063
pubs.acs.org/JACS

Electrochemical Formation of a *p*−*n* Junction on Thin Film Silicon Deposited in Molten Salt

Xingli Zou,[†,§] Li Ji,[†,‡,§] Xiao Yang,[†] Taeho Lim,[†] Edward T. Yu,[‡] and Allen J. Bard*[,†]

[†]Center for Electrochemistry, Department of Chemistry, The University of Texas at Austin, Austin, 78712 Texas, United States
[‡]Microelectronics Research Center, Department of Electrical and Computer Engineering, The University of Texas at Austin, Austin, 78758 Texas, United States

Supporting Information

ABSTRACT: Herein we report the demonstration of electrochemical deposition of silicon *p*−*n* junctions all in molten salt. The results show that a dense robust silicon thin film with embedded junction formation can be produced directly from inexpensive silicates/silicon oxide precursors by a two-step electrodeposition process. The fabricated silicon *p*−*n* junction exhibits clear diode rectification behavior and photovoltaic effects, indicating promise for application in low-cost silicon thin film solar cells.

Electricity generation via photovoltaic (PV) cells has attracted tremendous attention as it holds great promise to address worldwide environmental and energy issues.[1−13] Crystalline silicon PV cells will still likely dominate solar cell technology in the foreseeable future.[1−9,11−13] However, compared with fossil fuel-based electricity, the cost of silicon solar-based electricity is still too high.[2] Facile and low-cost production of solar Si cells remains a major challenge.[3,11] To drastically reduce the cost of manufacturing process for silicon solar cells, new alternatives are needed for production of solar silicon materials.

Thin film silicon solar cells have recently been intensively investigated due to their reduced material consumption,[2,8,13] but suffer from a complicated production process. Electrochemical method has been considered as a promising approach for the production of thin silicon films.[11,14] However, it is hard to electrochemically produce dense and high purity silicon film at low temperature due to its limited electrical conductivity.[15,16] Therefore, in recent years, electrodeposition of thin silicon film in molten salts has been proposed and investigated as a novel method to produce thin film silicon solar cells. Different molten salts, including fluoride- and chloride-based molten salts, have been investigated as electrolyte for the electrodeposition of silicon film. The major issue is to strictly control the impurity content in fluoride-based molten salts to produce high-purity silicon film.[17−19] Therefore, chloride-based molten salts have been recognized as promising electrolytes for the electrodeposition of high-purity silicon film.[20] The first photoactive *p*-type silicon film produced by electrodeposition in molten calcium chloride ($CaCl_2$) was demonstrated in our previous work.[21,22] The preliminary result exhibits 31% of the photocurrent response of a commercial *p*-type silicon wafer.[22] These results suggest promising potential in application for silicon thin film solar cells. In addition, compared with *de facto* technology for junction formation in industry, which involve multiple steps including $POCl_3$ diffusion, dopant drive-in and phosphosilicate glass removal,[23] *p*−*n* junction formation all by electrodeposition in molten salt will simplify the solar cell fabrication process with yielding a *p*−*n* junction directly from electrodeposition.

Here, we present the successful demonstration of silicon *p*−*n* junction electrodeposition in molten $CaCl_2$. Our results show that dense and homogeneous silicon thin films with embedded *p*−*n* junction can be deposited from inexpensive silicates/silicon oxide precursors through a two-step electrodeposition process. To the best of our knowledge, this is the first demonstration of a silicon *p*−*n* junction formed in molten salt. This work provides a novel approach to low-cost thin film solar cell production.

Molten salt electrodeposition processes provide a distinct opportunity for the production of crystalline silicon film, in which only electrons are consumed and silicates can be directly converted into silicon (Figure 1). High temperature is also beneficial to the crystallization of silicon films. In this work, inexpensive and abundantly available calcium silicate ($CaSiO_3$), calcium oxide (CaO) and silicon oxide (SiO_2) were used as precursors for the electrodeposition of silicon *p*−*n* junction film. The solubilities of $CaSiO_3$ and CaO in molten $CaCl_2$ at 850 °C are approximately 1.56 wt % and 20 mol %, respectively.[24] Therefore, $CaSiO_3$ and CaO were dissolved into molten $CaCl_2$ to form Ca^{2+}, SiO_3^{2-} and O^{2-}. Oxygen ions can further react with SiO_2 to form silicate ions (such as SiO_3^{2-} and SiO_4^{4-}, *etc.*),[24−26] which are silicate ions were reduced to silicon on the substrate to form silicon film. By using different dopants, *p*-type and *n*-type silicon films can be produced during electrodeposition, and thus a thin film silicon *p*−*n* junction can be produced by the two-step electrodeposition process (Figures 1b and S1). In a typical experiment, 100 g of $CaCl_2$, 1.0 g of $CaSiO_3$, 1.8 g of CaO and 1.4 g of SiO_2 were weighted and poured into a one-end closed quartz crucible, and then the crucible was placed into a one-end closed fused quartz tube in a furnace. After being heated up to 850 °C and kept at 850 °C in an argon gas atmosphere for 24 to 48 h, the electrodeposition experiment was then carried out by using a graphite plate as cathode substrate and a graphite rod/plate as anode (Figure 1a).

Received: August 25, 2017
Published: November 2, 2017

DOI: 10.1021/jacs.7b09090
J. Am. Chem. Soc. 2017, 139, 16060−16063

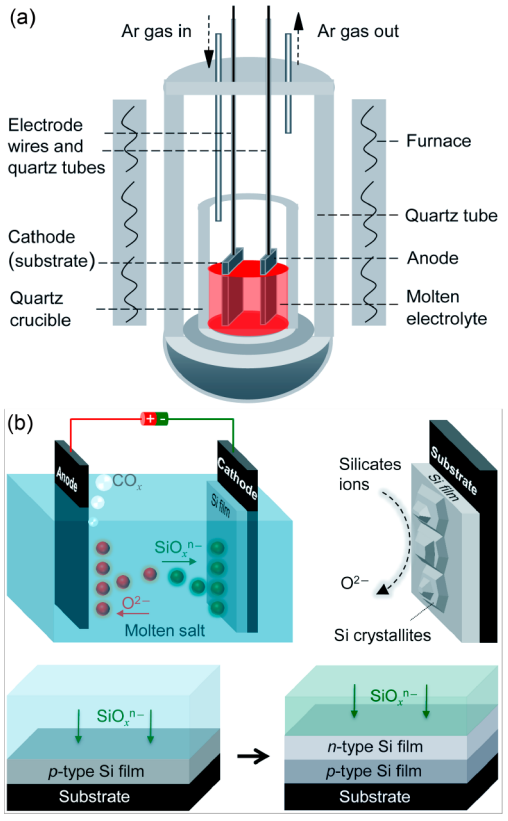

Figure 1. Schematic illustration of (a) the molten salt electrolytic cell and (b) the two-step electrodeposition process for fabricating thin film silicon $p-n$ junction.

Figure 2a shows the cyclic voltammogram (CV) curves of the electroreduction of calcium silicates on graphite in molten $CaCl_2$ containing $CaSiO_3/CaO/SiO_2$. The reduction of silicate ions starts at approximately −1.4 V versus a graphite pseudoreference electrode, and the oxidation of silicon starts at about −0.75 V. Typically, oxygen ions generated from CaO would react with SiO_2 to form different silicate ions, such as SiO_3^{2-}, SiO_4^{4-}, $Si_2O_7^{6-}$, *etc.*,[24−26] and all of these silicate ions would get reduced to silicon during electrodeposition. CaO serves as an intermediate medium to the continuous ionization of SiO_2 to form silicate ions, and thus the electrodeposition process for silicon film can proceed continuous (Figure S2). The electrodeposition process for the silicon film can be implemented via constant current density electrodeposition, constant potential electrodeposition or pulse electrodeposition processes. In this work, we demonstrate that the pulse electrodeposition process is beneficial to produce dense and smooth silicon film. The pulse electrodeposition condition is 120 s (current density: 15 mA cm $^{-2}$) for silicon electrodeposition and then 20 s (current density: 0) for the depletion layer to recover and bring silicate ions to the electrode surface, which means that the concentration of silicate ions in the reaction area kept at a relatively stable level. Figure 2b shows a typical potential-time plot of the pulse electrodeposition process for p-type silicon film. The electrodeposition process shows a constant variation trend. Stable electrodeposition process indicates the concentration of silicate ions is constant, which could contribute to form homogeneous silicon film, as shown in Figure 2c. The thickness of the film is about 40 μm, which generally depends on the deposition time. The faradaic efficiency for the formation of silicon film is approximately 60%, and the formation of silicon powders on the film may be mainly responsible for the remaining 40% efficiency. The growth rate of silicon film is not constant, which commonly decreases with time and also depends on current density and silicate ions concentration. Generally, a crystal silicon film with thickness of 5 to 50 μm can be produced in a controlled manner. Different current densities, potentials or pulse conditions could also result in different film morphologies.[21,22] The insets in Figure 2c are photos of the deposited p-type silicon film before and after being polished to form a mirror finish. If the surface of the deposited p-type silicon film is sufficiently smooth, the obtained

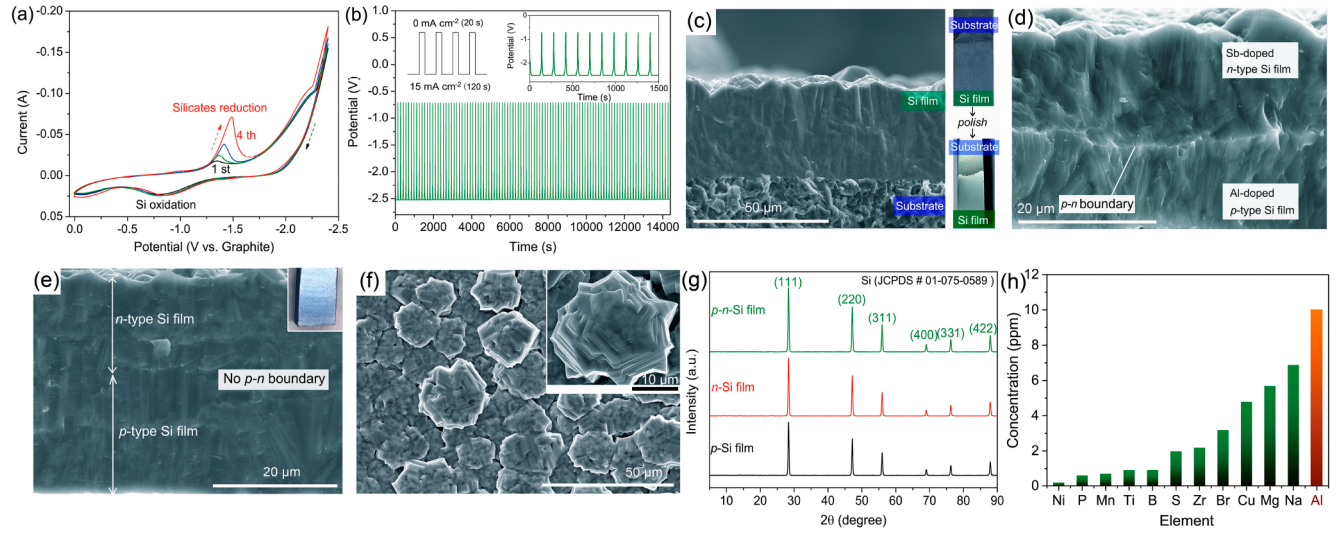

Figure 2. (a) Cyclic voltammetry (CV) curves of the molten $CaCl_2$ dissolved with $CaSiO_3/CaO/SiO_2$ at 850 °C (scan rate: 100 mV s $^{-1}$). (b) Typical potential-time curve of the first step: pulse electrodeposition of p-type silicon film. (c) Typical SEM image of the deposited p-type silicon film; the insets are photos of the silicon film before and after being polished. (d and e) Typical SEM images of the deposited silicon $p-n$ junction films (d) with and (e) without $p-n$ boundary; the inset in panel e is the photo of the polished $p-n$ junction film. (f) Typical SEM image of the surface of the deposited silicon film; the inset shows the details of a silicon particle. (g) Typical XRD patterns of the produced p-type, n-type and $p-n$ junction silicon films. (h) Glowing discharge mass spectrometry (GDMS) analysis of the produced silicon film.

DOI: 10.1021/jacs.7b09090
J. Am. Chem. Soc. 2017, 139, 16060−16063

thin films could be used directly (without being polished) as substrate to further electrodeposit *n*-type silicon film.

After polishing to render a mirror-like surface, the *p*-type silicon film was used as a substrate for *n*-type silicon deposition in a second electrolytic cell. The second electrolytic cell also composed of $CaCl_2$, $CaSiO_3$, CaO and SiO_2, and Sb_2O_3 was added into the bath to provide Sb as dopant for the *n*-type silicon film. The potential-time plot for *n*-type silicon deposition is similar to that of *p*-type. Figure 2d,e shows the scanning electron microscopy (SEM) images of the fabricated typical silicon *p*−*n* junction films. The *p* and *n* region can be distinguished via a clear boundary.

Figure S3 exhibits typical SEM images of the fabricated silicon *p*−*n* junction films with different thicknesses. Interestingly, the preferred crystal grown orientation of the *p*-type silicon film can be continuously maintained during the electrodeposition of *n*-type silicon film. With the *p*−*n* boundary gradually becoming homogeneous, a good *p*−*n* junction film can be thus fabricated. The thickness of the *p*-type silicon film and the *n*-type silicon film can be adjusted by changing experimental conditions. Generally, the thickness of the *p*−*n* junction film can reach up to 50 μm.

Figure 2f shows a typical SEM image of the surface of the produced silicon film. Typically, the *p*-type, *n*-type and *p*−*n* junction silicon films present similar surface morphology. The electrodeposited silicon films have dense and uniformly structure, and the size of the deposited silicon crystallites increases with the increase of electrodeposition time. The size of the silicon crystallites can reach up to about 30 μm. In addition, the crystallinity of the silicon film also increases with increasing electrodeposition time. The morphology of the silicon film can be well controlled to form a relatively smooth surface with small silicon crystallites or rough surface with larger silicon crystallites (Figures S4 and 2f). Figure 2g shows the X-ray diffraction (XRD) patterns of the produced silicon films including *p*-type silicon film, *n*-type silicon film and silicon *p*−*n* junction film, all of which exhibit good crystallinity.

Figure S5 depicts typical SEM images and EDS maps of the cross section of the produced *p*-type silicon film and silicon *p*−*n* junction film. Silicon is distributed uniformly in the silicon films; there are no obvious differences between the *p*-type silicon film and the silicon *p*−*n* junction film. Figure 2h shows results of glowing discharge mass spectrometry (GDMS) analysis of the produced silicon film, which confirms that impurity levels in the films are very low. The concentrations of B and P are both lower than 1 ppm. Other impurities except Ca and Cl are all less than 10 ppm (Figure S6). Ca and Cl may come from the residual $CaCl_2$ due to the insufficient water washing or from the entrapped molten salt at the grain boundaries. Depth profile of elemental analysis is required for further investigation. Other trace impurities such as Na, Mg, Ni, Ti and Zr are considered to derive from molten $CaCl_2$ and quartz crucible; these impurities influence the device performance of the silicon film. However, we postulate it is promising for further improvement of purity by using high-purity raw materials/quartz crucible and optimizing the operation. The element Al with 10 ppm concentration was considered as the *p*-type dopant for the silicon film. The Al was mainly derived from the quartz crucible (which contains 14 ppm Al) used in this investigation. To control the dopant concentration, additional alumina can be added into the molten salt to provide Al as dopant. For the *n*-type silicon film, it is proved that antimony or phosphorus can be used as the dopant in our system. However, the doping mechanism and the optimization of doping level are currently being investigated. The calculated diffusivities[27] for aluminum, antimony and phosphorus in silicon at 850 °C are shown in Figure S7. On the basis of the diffusivities, we postulate the thickness of the dopant diffusion layer between the *p*-type and *n*-type silicon films would be considerably less than the total thin film thicknesses, enabling formation of a *p*−*n* junction. These results show a great potential for the direct electrochemical production of high-quality silicon *p*−*n* junction film in molten salt for solar cells. Compare to the conventional multistep process, this short process direct from $SiO_2/CaSiO_3$ to a thin film silicon *p*−*n* junction may reduce the cost significantly.

The silicon *p*−*n* junction devices were then characterized by *I*−*V* measurements, under AM 1.5G, 1 sun illumination, with a 0.16 mm^2 aperture area. As shown in Figure 3a, the device

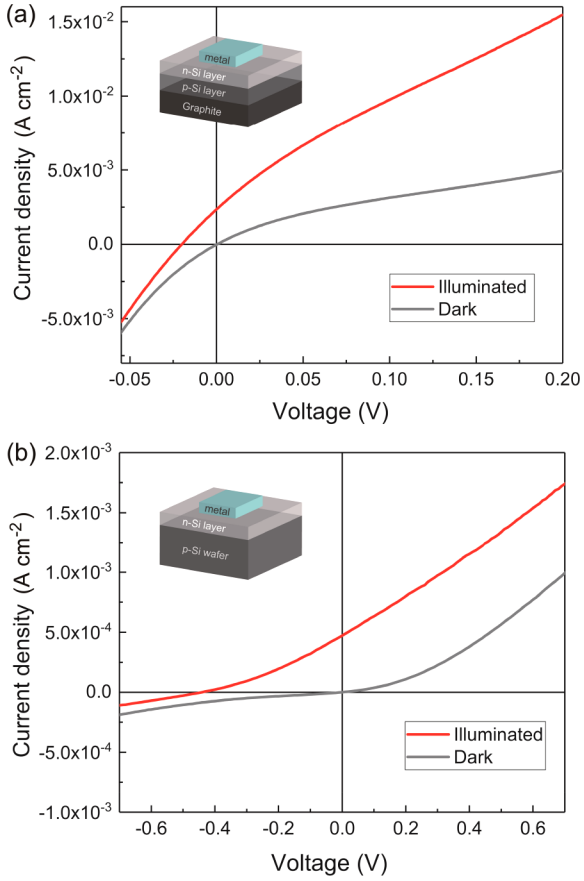

Figure 3. Current−voltage characteristics of (a) silicon *p*−*n* junction deposited in molten salt and (b) electrodeposited *n*-type silicon layer on *p*-type single crystalline silicon wafer, under dark (gray line) and under AM 1.5G, 1 sun illumination (red line), respectively.

under dark condition (gray line) shows reasonably good rectifying behavior, confirming the junction formation. When illuminated (red line), photocurrent and photovoltage are clearly observed, with 25 mV open-circuit potential.

To confirm the efficacy of *p*−*n* junction formation by a molten salt electrodeposition process, a Sb-doped *n*-type silicon layer was deposited on a *p*-type single crystalline wafer (~1 × 10^{16} cm^{-3}). As shown the *I*−*V* characterization in Figure 3b, 400 mV open-circuit potential is obtained, further demonstrating *p*−*n* junction can be formed in molten salt.

DOI: 10.1021/jacs.7b09090
J. Am. Chem. Soc. 2017, 139, 16060−16063

In summary, facile electrochemical deposition of thin film silicon $p-n$ junction in molten salt has been successfully demonstrated for the first time. Silicon $p-n$ junction film can be directly produced from inexpensive silicates/silicon oxide precursors through two-step electrodeposition process, which makes this technique attractive for low-cost manufacturing for silicon solar cells. Although the photovoltaic performance is currently modest, there is still a big margin for improving the overall film quality.

■ ASSOCIATED CONTENT

Supporting Information

The Supporting Information is available free of charge on the ACS Publications website at DOI: 10.1021/jacs.7b09090.

Experimental details, additional SEM, EDS, GDMS characterization data and the calculated diffusivity of dopants, *etc.* (PDF)

■ AUTHOR INFORMATION

Corresponding Author

*ajbard@cm.utexas.edu.

ORCID

Xingli Zou: 0000-0002-6608-8311

Allen J. Bard: 0000-0002-8517-0230

Author Contributions

§These authors contribute equally to this work

Notes

The authors declare no competing financial interest.

■ ACKNOWLEDGMENTS

This work was financially supported by the Global Climate and Energy Project (GCEP, Agreement No. 60853646-118146) and the Welch Foundation (F-0021)). This work was performed in part at the University of Texas Microelectronics Research Center, a member of the National Nanotechnology Coordinated Infrastructure (NNCI), which is supported by the National Science Foundation (grant ECCS-1542159). We sincerely appreciate Prof. Xionggang Lu (Shanghai University), Prof. Qian Xu (Shanghai University), Dr. Xiaole Chen (UT-Austin) and Niyi Mabayoje (UT-Austin) for the kind help, and Prof. Donald R. Sadoway (MIT), Prof. Cynthia Zoski (UT-Austin) and Dr. Eddie Forouzan (UT-Austin) for the valuable discussions.

■ REFERENCES

(1) Tian, B.; Zheng, X.; Kempa, T. J.; Fang, Y.; Yu, N.; Yu, G.; Huang, J.; Lieber, C. M. *Nature* **2007**, *449*, 885.

(2) Jeong, S.; McGehee, M. D.; Cui, Y. *Nat. Commun.* **2013**, *4*, 2950.

(3) Sun, K.; Shen, S.; Liang, Y.; Burrows, P. E.; Mao, S. S.; Wang, D. *Chem. Rev.* **2014**, *114*, 8662.

(4) Priolo, F.; Gregorkiewicz, T.; Galli, M.; Krauss, T. F. *Nat. Nanotechnol.* **2014**, *9*, 19.

(5) Bullock, J.; Hettick, M.; Geissbühler, J.; Ong, A. J.; Allen, T.; Sutter-Fella, C. M.; Chen, T.; Ota, H.; Schaler, E. W.; De Wolf, S.; Ballif, C.; Cuevas, A.; Javey, A. *Nat. Energy* **2016**, *1*, 15031.

(6) Garnett, E. C.; Yang, P. *J. Am. Chem. Soc.* **2008**, *130*, 9224.

(7) Powell, D. M.; Winkler, M. T.; Choi, H. J.; Simmons, C. B.; Needleman, D. B.; Buonassisi, T. *Energy Environ. Sci.* **2012**, *5*, 5874.

(8) Battaglia, C.; Cuevas, A.; De Wolf, S. *Energy Environ. Sci.* **2016**, *9*, 1552.

(9) Eisenberg, D.; Ahn, H. S.; Bard, A. J. *J. Am. Chem. Soc.* **2014**, *136*, 14011.

(10) Franzman, M. A.; Schlenker, C. W.; Thompson, M. E.; Brutchey, R. L. *J. Am. Chem. Soc.* **2010**, *132*, 4060.

(11) Poortmans, J.; Arkhipov, V. *Thin film solar cells: fabrication, characterization and applications*; Wiley: West Sussex, 2006.

(12) Branham, M. S.; Hsu, W.-C.; Yerci, S.; Loomis, J.; Boriskina, S. V.; Hoard, B. R.; Han, S. E.; Chen, G. *Adv. Mater.* **2015**, *27*, 2182.

(13) Mavrokefalos, A.; Han, S. E.; Yerci, S.; Branham, M. S.; Chen, G. *Nano Lett.* **2012**, *12*, 2792.

(14) Bard, A. J.; Faulkner, L. R. *Electrochemical methods: fundamentals and applications*; Wiley: New York, 2001.

(15) Shah, N. K.; Kumar Pati, R.; Ray, A.; Mukhopadhyay, I. *Langmuir* **2017**, *33*, 1599.

(16) Vlaic, C. A.; Ivanov, S.; Peipmann, R.; Eisenhardt, A.; Himmerlich, M.; Krischok, S.; Bund, A. *Electrochim. Acta* **2015**, *168*, 403.

(17) Haarberg, G. M.; Famiyeh, L.; Martinez, A. M.; Osen, K. S. *Electrochim. Acta* **2013**, *100*, 226.

(18) Yasuda, K.; Maeda, K.; Nohira, T.; Hagiwara, R.; Homma, T. *J. Electrochem. Soc.* **2016**, *163*, D95.

(19) Yasuda, K.; Maeda, K.; Hagiwara, R.; Homma, T.; Nohira, T. *J. Electrochem. Soc.* **2017**, *164*, D67.

(20) Cho, S. K.; Fan, F.-R. F.; Bard, A. J. *Electrochim. Acta* **2012**, *65*, 57.

(21) Cho, S. K.; Fan, F. R. F.; Bard, A. J. *Angew. Chem.* **2012**, *124*, 12912.

(22) Zhao, J.; Yin, H.; Lim, T.; Xie, H.; Hsu, H.-Y.; Forouzan, F.; Bard, A. J. *J. Electrochem. Soc.* **2016**, *163*, D506.

(23) Luque, A.; Hegedus, S. *Handbook of photovoltaic science and engineering*; John Wiley & Sons Ltd.: Chichester, 2003.

(24) Xiao, W.; Wang, X.; Yin, H.; Zhu, H.; Mao, X.; Wang, D. *RSC Adv.* **2012**, *2*, 7588.

(25) Xiao, W.; Jin, X.; Chen, G. Z. *J. Mater. Chem. A* **2013**, *1*, 10243.

(26) Zou, X.; Zheng, K.; Lu, X.; Xu, Q.; Zhou, Z. *Faraday Discuss.* **2016**, *190*, 53.

(27) Spit, F. H. M.; Albers, H.; Lubbes, A.; Rijke, Q. J. A.; Ruijven, L. J. V.; Westerveld, J. P. A.; Barker, H.; Radelaar, S. *Phys. Status Solidi A* **1985**, *89*, 105.

DOI: 10.1021/jacs.7b09090
J. Am. Chem. Soc. 2017, 139, 16060−16063